Published in final edited form as:
Brain Res. 2011 May 16; 1390: 41–49. doi:10.1016/j.brainres.2011.03.044.

Multiscale Imaging Characterization of Dopamine Transporter Knockout Mice Reveals Regional Alterations in Spine Density of Medium Spiny Neurons

M.L. Berlanga[a], **D.L. Price**[a,1], **B.S. Phung**[a], **R. Giuly**[a], **M. Terada**[a], **N. Yamada**[a], **M. Cyr**[b], **M.G. Caron**[b], **A. Laakso**[b,2], **M.E. Martone**[a], and **M.H. Ellisman**[a]

[a]National Center for Microscopy and Imaging Research, Center for Research in Biological Systems, University of California, San Diego, La Jolla, CA

[b]Department of Cellular Biology, Duke University Medical Center, Durham, NC

Abstract

The dopamine transporter knockout (DAT KO) mouse is a model of chronic hyperdopaminergia used to study a wide range of neuropsychiatric disorders such as schizophrenia, attention deficit hyperactivity disorder (ADHD), drug abuse, depression, and Parkinson's disease (PD). Early studies characterizing this mouse model revealed a subtle, but significant, decrease in the anterior striatal volume of DAT KO mice accompanied by a decrease in neuronal cell body numbers (Cyr et al., 2005). The present studies were conducted to examine medium spiny neuron (MSN) morphology by extending these earlier reports to include multiscale imaging studies using correlated light microscopy (LM) and electron microscopy (EM) techniques. Specifically, we set out to determine if chronic hyperdopaminergia results in quantifiable or qualitative changes in DAT KO mouse MSNs relative to wild-type (WT) littermates. Using Neurolucida Explorer's morphometric analysis, we measured spine density, dendritic length and synapse number at ages that correspond with the previously reported changes in striatal volume and progressive cell loss. Light microscopic analysis using Neurolucida tracings of photoconverted striatal MSNs revealed a highly localized loss of dendritic spines on the proximal portion of the dendrite (30 μm from the soma) in the DAT KO group. Next, thick sections containing MSN dendritic segments located at a distance of 20-60 μm from the cell soma, a region of the dendrite where spine density is reported to be the highest, were analyzed using electron microscope tomography (EMT). Because of the resolution limits of LM, the EM analysis was an extra measure taken to assure that our analysis included nearly all spines. Spine density measurements collected from the EMT data revealed only a modest decrease in the DAT KO group (n = 3 mice) compared to age-matched WT controls (n = 3 mice), a trend that supports the LM findings. Finally, a synaptic quantification using unbiased stereology did not detect a difference between DAT KO mice (n = 6 mice) and WT controls (n = 7 mice) at the EM level, supporting the focal nature of the early synaptic loss. These findings suggest that DAT KO mice have MSNs with highly localized spine loss and not an overall

Correspondence should be addressed to: Dr. Mark H. Ellisman and Dr. Monica L. Berlanga Tel: 1+(858)-534-0276 Fax: 1+(858)-534-7497 mark@ncmir.ucsd.edu (M. Ellisman), berlanga@ncmir.ucsd.edu (M. Berlanga) Postal Address: National Center for Microscopy and Imaging Research, Basic Sciences Bldg Room 1000, University of California, San Diego, 9500 Gilman Drive Dept Code 0608 La Jolla, California 92093-0608.

[1]Permanent address: ACADIA Pharmaceuticals Inc., 3911 Sorrento Valley Blvd., San Diego, CA 92121-1402

[2]Permanent address: Department of Neurosurgery, Helsinki University Central Hospital, Helsinki, Finland

morphologically distinct cell shape. The characterization of morphological changes in DAT KO mice may provide information about the neural substrates underlying altered behaviors in these mice, with relevance for human neurological disorders thought to involve altered dopaminergic homeostasis. Results from this study also indicate the difficulty in correlating structural changes across scales, as the results on fine structure revealed thus far are subtle and non-uniform across striatal MSNs. The complexities associated with multiscale studies are driving the development of shared online informatics resources by gaining access to data where it is being analyzed.

Keywords

electron tomography; striatum; bioinformatics; medium spiny neuron; morphometric analysis; spine density; cell centered database

1. Introduction

The dopamine transporter knockout (DAT KO) mouse lacks the plasma membrane dopamine transporter (DAT) protein that allows cells to recycle dopamine (DA) from extracellular space (Giros et al., 1996). As a result, DA clearance from the synaptic cleft is greatly reduced, resulting in a 5-fold increase in extracellular levels of DA (Gainetdinov et al., 1998) but a marked reduction of DA in vesicles of DA neurons (Jones et al., 1998). In this mouse model, extracellular DA availability is high in the striatum and can lead to prolonged activation of DA receptors or altered pre- and post-synaptic DA receptor expression and function (Dumartin et al., 2000; Fauchey et al., 2000; Giros et al., 1996; Jones et al., 1998). Dopamine receptor-mediated behavioral abnormalities exhibited by the DAT KO mouse include elevated baseline locomotor activity (Giros et al., 1996), prepulse inhibition deficits of the startle response (Ralph et al., 2001), and deficits in executive function (Morice et al., 2007). The behavioral disturbances exhibited by these mice may reflect underlying differences in their neurocircuitry, as a result of their chronically elevated extracellular DA levels. Accordingly, striatal cell loss (Cyr et al., 2005) as well as changes in projections from the prefrontal cortex to the mesocortical limbic system have been observed (Zhang et al., 2010) suggesting a functional reorganization of striatal cell circuits.

DAT KO mice have a 5-fold increase in basal extracellular DA concentrations (Gainetdinov et al., 1998; Jones et al., 1998) and exhibit 5-6 times more locomotor activity than wild-type (WT) animals (Giros et al., 1996). Repeated administration of cocaine or amphetamine also produces a hyperdopaminergic state in the striatum causing increases in locomotor activity, similar to the DAT KO mouse, and, thus, the DAT KO mouse is a putative animal model for long-term drug use (Jones et al., 1998). The hyperdopaminergic state induced by long-term drug use has been shown to cause robust morphological changes in the cellular networks of striatal medium spiny neurons (MSNs) (Lee et al., 2006; Robinson and Kolb, 1999). A detailed examination of striatal cell morphology in the DAT KO mouse has not previously been reported. Therefore, the present study analyzed the morphology of MSNs from the DAT KO mouse and WT littermate controls using correlated light microscopy (LM) and electron microscopy (EM) techniques to determine whether quantifiable or qualitative neuroadaptive changes in MSNs were taking place as a result of the chronic hyperdopaminergic environment that is known to exist in the striatum of this mouse model.

Although spine density measurements are typically quantified at the LM level using classical Golgi staining, photoconversion of Lucifer yellow was used in the present study to isolate a single cell and its entire dendritic field so that dendritic segments (analyzed in thick sections for EM) could be successfully mapped back to the original neuron for correlated analysis at the EM level. Furthermore, a comparison of previous LM and EM studies (Gioia

et al., 1998; Harris and Stevens, 1988) on spine density demonstrates that spine density quantifications at the LM level typically underestimate spine measurements at the EM level. Because the photoconverted MSNs traced and analyzed in this study are susceptible to the same resolution limits at the LM level as classical Golgi staining, these neurons were further processed for analysis at the EM level, to ensure that many spines were not going undetected.

This project is an extension of earlier studies examining magnetic resonance imaging (MRI) volumes of DAT KO animals. These studies reported that a decrease in the volume of the anterior striatum in DAT KO mice correlated to a loss in neuron number as compared to age-matched controls (Cyr et al., 2005). Such changes at the cellular level suggest that alterations in the striatal microcircuitry may also be occurring. This reduction in neuron numbers could translate into changes in dendritic sprouting, synapse number, and overall synaptic connectivity known to accompany alterations in cell morphology (Holtmaat et al., 2008; Knott et al., 2006). Changes in cell morphology can also come about as a result of increases in DA neurotransmission (Lee et al., 2006). Giros et al. previously reported that extracellular DA persists 100 times longer in DAT KO mice (1996). Therefore, prolonged alterations in DA receptor expression and/or function likely persist as well. In fact, some DA receptors target synaptic scaffolding proteins and other structurally-related cytoskeletal proteins (Allen et al., 2006). Thus, prolonged DA availability in DAT KO mice could potentially induce changes in cell morphology in DA-rich brain areas, such as the striatum.

Based on the previous reports of cellular changes in the DAT KO mouse, and the effects of DA on dendritic structures mediating synaptic transmission in striatal MSNs, we conducted a detailed structural investigation of MSNs using correlated LM and EM to investigate whether quantitative or qualitative alterations in MSN spine density, dendritic length and synapse number were taking place in addition to the striatal cell loss previously reported in the DAT KO mouse.

2. Results

2.1 Correlated light and electron microscopy

Figure 1 shows representative Neurolucida tracings of MSNs from DAT KO and WT mice. Neurons were analyzed in Neurolucida Explorer 4.0 using an enhanced 3D Sholl analysis, which we will refer to as the morphometric analysis (to avoid any confusion with the traditional 2D Sholl analysis). Differences in spine density and dendritic length were measured in 10 μm increments away from the cell body to the most distal regions of the dendrites. The morphometric analysis revealed a significant decrease ($p = 0.041$) in spine density in the DAT KO group ($n = 5$ mice) at 30 μm away from the soma compared to the age-matched control group ($n = 7$ mice) [Figure 2]. No significant differences in dendritic length or number of dendritic intersections were detected between groups [Figure 3 and Figure 4]. Furthermore, the cell traces showed no significant difference in the number of primary dendrites between groups [Figure 5].

Subsequently, dendritic segments from the same cells analyzed in the morphometric analysis were selected at a distance of 20-60 μm from the cell soma and analyzed using electron microscopic tomography (EMT). Figure 6 shows a 3D model of a dendritic segment from a DAT KO mouse and a WT mouse. Electron microscope tomography data showed a modest decrease ($t = -2.3590$, $p = 0.0778$) in spine number per unit surface area in the DAT KO group ($n = 3$ mice) compared to the WT controls ($n = 3$ mice) [Figure 7]. No significant differences were found in surface area or length of dendritic segments analyzed in each group (data not shown).

2.1.1 Synaptic Quantification—A synaptic quantification using unbiased stereology revealed no significant differences between the synapse to neuron ratio in the striatum of DAT KO (n = 6 mice) and WT (n = 7 mice) groups [Figure 8], where neuron density was found to be stable (neuron density$_{WT}$ = 329602.8853 ± 30102.29574 neurons/mm^3 and neuron density$_{KO}$ = 324371.1461 ± 42240.50977 neurons/mm^3) [Figure 9].

3. Discussion

Localized differences in striatal MSN spine densities between DAT KO mice and WT controls were identified in this study using correlated LM and EM techniques. Results from this multiscale study indicate that at the LM and EM levels, striatal MSNs of the DAT KO mouse exhibit highly localized spine loss on the proximal portions (30 μm away from cell body) of their dendritic trees when compared to WT mice and no overall distinct cell shape. In addition, the synaptic connectivity of the striatum does not show any robust reorganization, which has been previously found in the nucleus accumbens, a subregion of the striatum, following chronic drug-induced hyperdopaminergia (Alcantara et al., 2011).

Previous studies examining the synaptic organization of the striatum show that local interneurons and other MSNs form synapses along the proximal portions of these spiny dendrites (Groenewegen et al., 1991; Smith and Bolam, 1990; Wilson, 2004). Therefore, this significant reduction in spine density may indicate a selective loss in the number of local synaptic connections specifically onto the MSNs (i.e. the projection neurons) of the striatum in the DAT KO mouse. In further support of this notion is the previous observation by Cyr et al., where a decrease in striatal neuron number accompanied an overall decrease in striatal volume (2005).

Spine density changes in the present study were analyzed with respect to distance from the soma because spine changes are not always uniform along the length of the dendrite (Li et al., 2003; Robinson and Kolb, 1999). This is especially true when dealing with dendrites that travel through different layers, as in the cortex for example, where the source of axonal projections can vary from layer to layer. Although the striatum does not have distinct layers, it is organized into patch-matrix compartments whose boundaries are maintained by local neurons and afferent fibers (Ragsdale and Graybiel, 1981). Moreover, it has been shown that synaptic inputs onto MSN dendrites do maintain a certain level of organization. Cortical and thalamic synapses tend to synapse onto distal portions of the MSN dendrites, whereas local striatal neurons synapse on proximal portions of MSN dendrites (Groenewegen et al., 1991; Smith and Bolam, 1990). The cortical and thalamic inputs are thought to be mediated by nearby dopaminergic synapses made onto the spine head, spine stalk, or dendritic shaft (Freund et al., 1984). Furthermore TH-positive nerve terminals make up only 3% of the total synaptic density in the DA-rich striatum (Roberts et al., 2002); consequently, DA transmission and receptor activation in the striatum is thought to be largely accomplished via volume transmission. This further supports the notion that the localized spine loss observed in this study may not be a direct effect of DA, but a result of fewer local striatal neurons.

From a functional stand point, the selective spine loss close to the cell body could alter synaptic integration of the MSNs. Since the MSNs are the primary projection neurons of the striatum, such altered synaptic connectivity could affect the overall output of the striatum, perhaps even explain some of the striatum-related behavioral abnormalities associated with this mouse model.

The DAT KO mouse model has been suggested for use in studying the long-term effects of chronic hyperdopaminergia in drug dependence. For example, chronic cocaine or amphetamine use (passive or self-administered) results in increased extracellular DA in the

striatum (Lecca et al., 2007). This chronic drug-induced hyperdopaminergia leads to robust increases in spine density on the distal portion of dendrites of MSNs (Lee et al., 2006; Li et al., 2003; Robinson and Kolb, 1999), as well as an increase in the synapse to neuron ratio in striatal subregions (Alcantara et al., 2011). Such increases in spine density and synaptic reorganization were not observed on the distal portion of dendrites of striatal MSNs in the DATKO mouse, the model of hyperdopaminergia used in this study; however, in agreement with the current findings, Robinson and Kolb (1999) do report a significant decrease in spine density on proximal dendrites of MSNs.

Thus, there appears to be some differences in the types of long-term changes induced by these two chronic hyperdopaminergic environments. One possible explanation is that the DAT KO mouse may undergo developmental neuroadaptations that compensate for the absence of the DAT in a stable hyperdopaminergic environment as compared to the repetitive temporary DA surges caused by cocaine or amphetamine in the striatum of a fully developed animal. Mechanisms underlying such contrasting long-term effects of DA require further exploration.

4. Materials and Methods

4.1 Subjects

Male and female DAT KO mice (n = 11) and wild-type (WT) littermates (n = 14) 6-7 months old were used in this study. This line of mice has been described previously (Giros et al., 1996). The mice were housed in an AAALAC (Association for Accreditation of Laboratory Animal Care, International) accredited animal care facility on a 12 hour light/dark cycle with food and water provided ad libitum. Animal care was in accordance with the Guide for Care and Use of Laboratory Animals (NIH publication 865-23, Bethesda, MD) and approved by the Institutional Animal Care and Use Committee.

4.1.1 Tissue preparation—Animals were deeply anesthetized with an interperitoneal injection of pentobarbital (10 mg/g body weight). Next, mice were perfused transcardially with oxygenated Ringer's solution at 37°C (0.79% NaCl, 0.038% KCl, 0.20% $MgCl_26H_2O$, 0.018% $NaHPO_4$, 0.125% $NaCHO_3$, 0.03% $CaCl_22H_2O$, 0.20% dextrose, and 0.02% xylocaine) for ~30 seconds, followed by 0.1M PBS, pH 7.4 containing 4% paraformaldehyde and 0.1% glutaraldehyde (37°C) for 10 minutes. The mouse brain was removed and stored in same fixative for 2 hours. Five DAT KO and 7 WT mice were used for the correlated light and electron microscopic studies. The brains were divided into hemispheres and coronal sections were collected using a Vibratome (VT1000E, Leica Microsystems, Wetzlar, Germany). The left hemisphere was sectioned into100 μm-thick sections for the intracellular injections with Lucifer yellow. The right hemisphere was sectioned into 70 μm-thick sections and placed in cryoprotectant. Later, a second cohort of animals, 6 DAT KO and 7 WT mice, were perfused using the same methods described above, and the tissue was processed using conventional EM techniques for the synaptic quantification.

4.1.2 Intracellular fills of medium spiny neurons—The 100 μm-thick slices were stored in ice-cold PBS and used immediately. The slices were placed in cold PBS and viewed with an Olympus Optical (Melville, NY) BX50WI infrared differential interference contrast (DIC)/epifluorescent microscope, using a 60x water immersion objective. Sharp glass micropipettes were pulled on a vertical pipette puller (David Kopf Instruments, Tujunga, CA) using omega-dot capillary tubes (outer diameter of 1.00 mm and inner diameter of 0.58 mm; resistances ranged between 100 and 400 MΩ) and backfilled with 5% aqueous dilithium Lucifer yellow CH (LY) (Calbiochem, La Jolla, CA). Medium spiny

neurons in the dorsal lateral and ventral medial quadrants of the striatum were injected with Lucifer Yellow. The somata were impaled, and the dye was injected into the cells by applying a 0.5 sec negative current pulse (1 Hz) until the processes were completely filled. The medium spiny neurons were identified by the size and shape of their soma (10-15 μm in diameter), and, once injected, the presence of dendritic spines. After several cells were filled in a tissue slice, the slice was then placed in 2% glutaraldehyde–PBS for 30 min at 4°C, followed by processing for photooxidation.

4.1.3 Photooxidation of Lucifer yellow-filled medium spiny neurons—To examine neurons at the EM level, dye-filled MSNs were photooxidized as described previously (Deerinck et al., 1994). Briefly, the slices were rinsed with 1X PBS and then placed in PBS containing 0.38% glycine for 2 min. They were again rinsed in PBS and then placed in oxygenated PBS containing 0.1% potassium cyanide and 0.15% diaminobenzidine (DAB). After incubating in the DAB solution for 5 min, the LY-filled MSN was exposed to intense illumination using a 75 W xenon lamp and a fluorescein excitation filter. The DAB solution was periodically replaced with freshly oxygenated solution during the process of photoconversion. When LY fluorescence was extinguished and the cell and its dendritic processes were distinctly brown, the illumination was terminated, and the slice was washed three times for 10 min in ice-cold PBS. The slices were subsequently processed for EM.

4.1.4 Preparation of conventionally fixed and embedded samples—Vibratome sections were osmicated in sodium cacodylate buffered 1% OsO4 for 1 hour. After three 5 minute rinses with double distilled water, the slices were dehydrated with an ethanolic series (50, 70, 90, and 100%), followed by dry acetone (2 times, 5 minutes each). The slices were infiltrated with a solution of 50% acetone–50% Durcupan ACM epoxy resin (Electron Microscopy Sciences, Ft. Washington, PA) for 1 hour, and then with 100% resin (overnight). The following day the slices were placed into fresh Durcupan and placed on a rotator for 1 hour. The slices were flat embedded by placing them between two mold-release-coated slides and left at 60°C for 48 hr.

4.1.5 Light microscopy and morphometric analysis—Photooxidized cells embedded in epoxy resin were imaged using a Bio-Rad Radiance 2000 Confocal/2-Photon microscope. A digital volume of each cell was collected using Laser Sharp 2000™ software (BioRad Cell Science Division, Hemel Hempstead, UK) and cells were traced using Neurolucida 8.0 (MBF Biosciences, Williston, VT). Three-dimensional views of cells were checked for accuracy using custom made software ViQI (developed at NCMIR). Cell tracings were analyzed in Neurolucida Explorer and using the morphometric analysis provided in the Neurolucida Explorer 4.0 software package. The morphometric analysis provided in this software package is a 3D Sholl analysis using concentric spheres with a distance of 10 μm between each sphere. The smallest sphere is centered within the soma. The parameters that were analyzed included: spine density, total dendritic length, and number of dendritic intersections.

4.1.6 Sectioning and analysis for electron microscopy of conventionally fixed specimens—An area of striatum with dimensions 0.5 by 0.5 mm was excised from conventionally prepared samples and glued to an acrylic rod for thin (70 nm thick) and thick (500 nm thick) sectioning using a diamond knife (Diatome) and an ultramicrotome (Reichert Ultracut E). The striatal regions were selected to match the locations of the photoconverted MSNs used in the UHVEM portion of the study. Thin sections were imaged at 80 kV using a JEOL 1200 electron microscope and thick sections were dried onto a glass slide, stained with toluidene blue, and imaged on a computer-assisted Olympus DSU microscope

(Olympus, Essex, UK) equipped with, Microfire camera, and an automated XYZ stage for mosaic imaging using Neurolucida software (MBF Biosciences, Williston, VT).

The physical disector method was used to estimate the synapse-to-neuron ratio calculated from neuronal density and synapse density (Gundersen et al., 1988; Sterio, 1984). Neuron density was measured using the semithin sections and synapse density was calculated using the ultrathin sections. Semithin sections and ultrathin sections were collected from the same block of tissue using an ultramicrotome. Cells and synapses were each counted manually by one observer blind to group assignment using the unbiased quantitative stereological physical disector method.

Neuron density was calculated by dividing the number of cells counted by the volume of the tissue which involved comparing every other section (0.5 μm-thick) in a series of twenty sections (Gundersen et al., 1988; Sterio, 1984) stained with toluidene blue. Each section was dried onto a glass slide and stained with toluidene blue. Ten sections were imaged on an Olympus microscope (DSU) using a precision mosaic imaging stage for image acquisition of each section. The first section was designated the Reference section and the second was the Lookup section. The second section then became the Reference section for the third section and so on, using a total of ten semithin sections. When a cell nucleus was found in the Reference section, but not the Lookup section, the nucleus was counted. Within an unbiased counting frame (A_{frame}) of a known area (54,600 μm^2 at 40x for semithin sections) the number of nuclei that were present in the Reference section and not in the Lookup section was counted (Q^-_{neuron}). Next the volume of tissue through which the cells were counted (V_{dis}) was calculated using the following formula: $V_{dis}=A_{frame} \times H$, where H is section thickness (1μm) multiplied by the number of sections. The neuronal density, Nv_{neuron}, was then determined by dividing the number of cells counted by the volume of the tissue using the following formula: $Nv_{neuron} = Q^-_{neuron}/V_{dis}$ (using semithin sections).

Synapse density was determined using a ribbon of 10 ultrathin (70 nm) serial sections which was collected onto a Formvar-covered slot grid. Grids were post stained with 1% uranyl acetate (aqueous) and a picture of the same location on each section (one image per section) was acquired on film at 80 kV using a JEOL 1200 electron microscope.

4.1.7 Sectioning and segmentation for electron tomography of photooxidized cells—Photooxidized cells were excised from resin-embedded tissue sections and glued onto an acrylic rod for sectioning on an ultramicrotome. Serial sections were collected at 3-4 μm-thick, placed in warm water to flatten sections, and subsequently examined under a light microscope. Sections with the longest photooxidized dendritic segments were collected onto 50-50 clamshell mesh grids. Gold beads 5 and 10 nm in diameter were applied to the top (5 nm) and bottom (10 nm) of each section prior to imaging. Materials were sent to Osaka University in Japan for imaging at 3 MV on the ultra high voltage electron microscope (UHVEM). A 60 degree tilt series for each dendritic segment was acquired digitally or on film and the images were shipped back to NCMIR for processing and analysis. Image processing of a tilt series included backprojection reconstruction of the volume followed by segmentation of the dendritic segment using IMOD version 3.9 (http://bio3d.colorado.edu/imod/). Once each segmentation was complete, the numerical data was exported from IMOD into an Excel spreadsheet. Values regarding spine number, surface area of the dendritic shaft, and spine classification were analyzed in Excel (Microsoft Office 2007).

4.1.8 Electron tomographic reconstruction—Tilt series for each dendritic segment were aligned using IMOD for fiducial alignment and data manipulations prior to generating back projection. Back projection was performed using the TxBr package (Lawrence et al.,

2006). Dendritic shaft and spines were traced for each dendritic segment in IMOD and 3D views were generated by using the meshing tool in IMOD. Surface area measurements for each dendritic shaft and all spines were calculated in IMOD.

4.1.9 Statistical Analyses—Data from the morphometric analysis and EMT reconstructions was entered into Excel spreadsheets and a mixed effects-regression-based version of a two-sample comparison was used to determine significant differences between the DAT KO and WT groups.

Data from the synaptic quantification was entered into an excel spreadsheet and analyzed using SigmaPlot 10. A two-tailed t-test was used to measure differences in the synapse to neuron ratio between DAT KO and WT groups.

4.2.0 Data deposition—Tomographic reconstructions, 3D models and animations of dendritic segments from all animals used in this study are available upon publication in the Cell Centered Database (CCDB) (Martone et al., 2002; Martone et al., 2003). All of the data for this project can be found at: http://ccdb.ucsd.edu by searching under the project ID# P1207.

5. Conclusions

The present multiscale imaging study points to phenotypic differences between medium spiny neurons (MSNs) in DAT KO and WT mice. Using correlated LM and EM techniques, we found highly localized alterations in MSN spine density in this animal model of hyperdopaminergia. A closer examination of the types of morphological differences in the MSNs of DAT KO mice compared to WT animals will help researchers better understand the neural basis for behavioral abnormalities associated with this mouse model. Moreover, if the localized morphological changes reported in this study are in fact a downstream effect of local reorganization within the striatum and not a consequence of direct DA action, such identified neuroadaptive changes could elucidate some of the non-specific actions of DA on cell morphology in a hyperdopaminergic mouse model. Such findings could extend to other human-related clinical disorders such as schizophrenia and drug dependency.

Lastly, electron tomography studies generate large volumes of data. Thus, one challenge when processing data from the present correlated LM and EM study was learning how to handle the volume of data generated from a project of such large magnitude. In addition, correlating the quantitative findings between the LM and EM levels sheds light not only on the inherent challenges associated with this type of multiscale analysis, but the difficulty in general when comparing data across scales. Such complexities associated with this kind of multiscale and multimodal analysis demonstrate the value in a shared public resource for depositing image data and relevant metadata. Therefore, all of the raw data obtained in the conduct of this work are now available at: http//www.ccdb.ucsd.edu/index.shtm, to help researchers with data accessibility for data comparison of any current or future studies related to this subject.

Acknowledgments

This work was supported by NCRR RR04050 (MHE), NIDA DA 016602 (MEM), NIH AG000216, NCRR RR043050 (MHE), NINDS NS 19576 (MC) and NIDA DA13511 (MC). The authors wish to thank Andrea Thor for her assistance with sectioning, Brian Kang, Kenny Lam, Isabel Alegria, Justin Yeap for their assistance with cell tracing and EMT segmentation, Steve Lamont, Natalie MacLean, James Obayashi, Van Phung and William Smith, for their technical assistance.

References

Alcantara AA, Lim HY, Floyd CE, Garces J, Mendenhall JM, Lyons CL, Berlanga ML. Cocaine- and morphine-induced synaptic plasticity in the nucleus accumbens. Synapse. 2011; 65:309–20. [PubMed: 20730804]

Allen PB, Zachariou V, Svenningsson P, Lepore AC, Centonze D, Costa C, Rossi S, Bender G, Chen G, Feng J, Snyder GL, Bernardi G, Nestler EJ, Yan Z, Calabresi P, Greengard P. Distinct roles for spinophilin and neurabin in dopamine-mediated plasticity. Neuroscience. 2006; 140:897–911. [PubMed: 16600521]

Cyr M, Caron MG, Johnson GA, Laakso A. Magnetic resonance imaging at microscopic resolution reveals subtle morphological changes in a mouse model of dopaminergic hyperfunction. Neuroimage. 2005; 26:83–90. [PubMed: 15862208]

Deerinck TJ, Martone ME, Lev-Ram V, Green DP, Tsien RY, Spector DL, Huang S, Ellisman MH. Fluorescence photooxidation with eosin: a method for high resolution immunolocalization and in situ hybridization detection for light and electron microscopy. J Cell Biol. 1994; 126:901–10. [PubMed: 7519623]

Dumartin B, Jaber M, Gonon F, Caron MG, Giros B, Bloch B. Dopamine tone regulates D1 receptor trafficking and delivery in striatal neurons in dopamine transporter-deficient mice. Proc Natl Acad Sci U S A. 2000; 97:1879–84. [PubMed: 10677550]

Fauchey V, Jaber M, Caron MG, Bloch B, Le Moine C. Differential regulation of the dopamine D1, D2 and D3 receptor gene expression and changes in the phenotype of the striatal neurons in mice lacking the dopamine transporter. Eur J Neurosci. 2000; 12:19–26. [PubMed: 10651856]

Freund TF, Powell JF, Smith AD. Tyrosine hydroxylase-immunoreactive boutons in synaptic contact with identified striatonigral neurons, with particular reference to dendritic spines. Neuroscience. 1984; 13:1189–215. [PubMed: 6152036]

Gainetdinov RR, Jones SR, Fumagalli F, Wightman RM, Caron MG. Reevaluation of the role of the dopamine transporter in dopamine system homeostasis. Brain Res Brain Res Rev. 1998; 26:148–53. [PubMed: 9651511]

Gioia M, Tredici G, Bianchi R. Dendritic arborization and spines of the neurons of the cat and human periaqueductal gray: a light, confocal laser scanning, and electron microscope study. Anat Rec. 1998; 251:316–25. [PubMed: 9669758]

Giros B, Jaber M, Jones SR, Wightman RM, Caron MG. Hyperlocomotion and indifference to cocaine and amphetamine in mice lacking the dopamine transporter. Nature. 1996; 379:606–12. [PubMed: 8628395]

Groenewegen, H.; Berendse, H.; Meredith, G.; Haber, S.; Voorn, P.; JG, W. Functional anatomy of the ventral limbic system-innervated striatum. In: Willner, P.; Scheel-Kruger, J., editors. The Mesolimbic Dopamine System: From Motivation to Action. John Wiley & Sons; New York: 1991. p. 19-59.

Gundersen HJ, Bagger P, Bendtsen TF, Evans SM, Korbo L, Marcussen N, Moller A, Nielsen K, Nyengaard JR, Pakkenberg B, et al. The new stereological tools: disector, fractionator, nucleator and point sampled intercepts and their use in pathological research and diagnosis. APMIS. 1988; 96:857–81. [PubMed: 3056461]

Harris KM, Stevens JK. Dendritic spines of rat cerebellar Purkinje cells: serial electron microscopy with reference to their biophysical characteristics. J Neurosci. 1988; 8:4455–69. [PubMed: 3199186]

Holtmaat A, De Paola V, Wilbrecht L, Knott GW. Imaging of experience-dependent structural plasticity in the mouse neocortex in vivo. Behav Brain Res. 2008; 192:20–5. [PubMed: 18501438]

Jones SR, Gainetdinov RR, Jaber M, Giros B, Wightman RM, Caron MG. Profound neuronal plasticity in response to inactivation of the dopamine transporter. Proc Natl Acad Sci U S A. 1998; 95:4029–34. [PubMed: 9520487]

Knott GW, Holtmaat A, Wilbrecht L, Welker E, Svoboda K. Spine growth precedes synapse formation in the adult neocortex in vivo. Nat Neurosci. 2006; 9:1117–24. [PubMed: 16892056]

Lawrence A, Bouwer JC, Perkins G, Ellisman MH. Transform-based backprojection for volume reconstruction of large format electron microscope tilt series. J Struct Biol. 2006; 154:144–67. [PubMed: 16542854]

Lecca D, Cacciapaglia F, Valentini V, Acquas E, Di Chiara G. Differential neurochemical and behavioral adaptation to cocaine after response contingent and noncontingent exposure in the rat. Psychopharmacology (Berl). 2007; 191:653–67. [PubMed: 16932924]

Lee KW, Kim Y, Kim AM, Helmin K, Nairn AC, Greengard P. Cocaine-induced dendritic spine formation in D1 and D2 dopamine receptor-containing medium spiny neurons in nucleus accumbens. Proc Natl Acad Sci U S A. 2006; 103:3399–404. [PubMed: 16492766]

Li Y, Kolb B, Robinson TE. The location of persistent amphetamine-induced changes in the density of dendritic spines on medium spiny neurons in the nucleus accumbens and caudate-putamen. Neuropsychopharmacology. 2003; 28:1082–5. [PubMed: 12700699]

Martone ME, Gupta A, Wong M, Qian X, Sosinsky G, Ludascher B, Ellisman MH. A cell-centered database for electron tomographic data. J Struct Biol. 2002; 138:145–55. [PubMed: 12160711]

Martone ME, Zhang S, Gupta A, Qian X, He H, Price DL, Wong M, Santini S, Ellisman MH. The cell-centered database: a database for multiscale structural and protein localization data from light and electron microscopy. Neuroinformatics. 2003; 1:379–95. [PubMed: 15043222]

Morice E, Billard JM, Denis C, Mathieu F, Betancur C, Epelbaum J, Giros B, Nosten-Bertrand M. Parallel loss of hippocampal LTD and cognitive flexibility in a genetic model of hyperdopaminergia. Neuropsychopharmacology. 2007; 32:2108–16. [PubMed: 17342172]

Ralph RJ, Paulus MP, Fumagalli F, Caron MG, Geyer MA. Prepulse inhibition deficits and perseverative motor patterns in dopamine transporter knock-out mice: differential effects of D1 and D2 receptor antagonists. J Neurosci. 2001; 21:305–13. [PubMed: 11150348]

Roberts RC, Force M, Kung L. Dopaminergic synapses in the matrix of the ventrolateral striatum after chronic haloperidol treatment. Synapse. 2002; 45:78–85. [PubMed: 12112400]

Robinson TE, Kolb B. Alterations in the morphology of dendrites and dendritic spines in the nucleus accumbens and prefrontal cortex following repeated treatment with amphetamine or cocaine. Eur J Neurosci. 1999; 11:1598–604. [PubMed: 10215912]

Smith AD, Bolam JP. The neural network of the basal ganglia as revealed by the study of synaptic connections of identified neurones. Trends Neurosci. 1990; 13:259–65. [PubMed: 1695400]

Sterio DC. The unbiased estimation of number and sizes of arbitrary particles using the disector. J Microsc. 1984; 134:127–36. [PubMed: 6737468]

Wilson, CJ. The Synaptic Organization of the Brain. Shepherd, GM., editor. Oxford University Press, Inc.; Oxford: 2004. p. 361-414.

Zhang X, Bearer EL, Boulat B, Hall FS, Uhl GR, Jacobs RE. Altered neurocircuitry in the dopamine transporter knockout mouse brain. PLoS One. 2010; 5:e11506. [PubMed: 20634895]

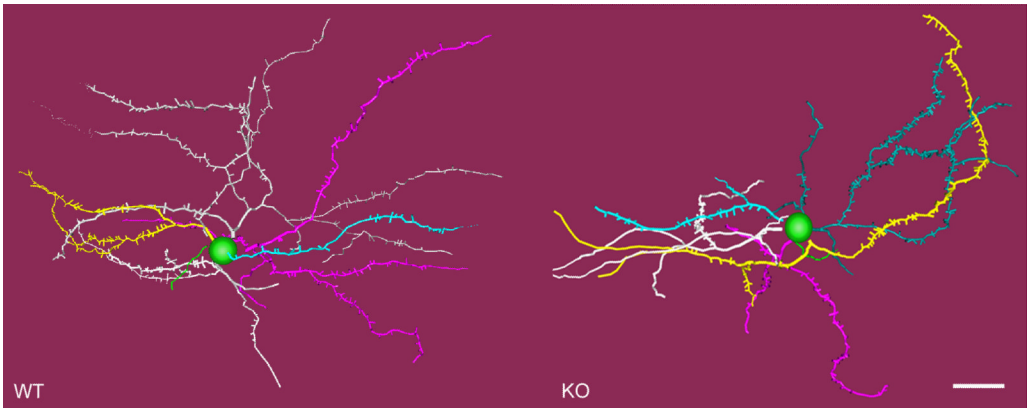

Figure 1. 3D renderings of photoconverted medium spiny neurons (MSNs)

Data from cell tracings of photoconverted cells were gathered using Neurolucida Explorer. WT and KO cell tracings were then rendered in 3D using ViQI. [Scale bar = 15 microns; WT = wild-type; KO = dopamine transporter knockout].

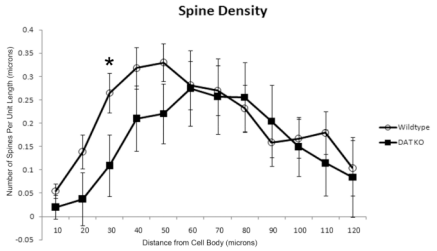

Figure 2. Striatal MSN spine density is reduced in DAT KO mice

Spine density measurements collected from a morphometric analysis comparing WT and KO animals. Graph shows a significant reduction in spine density (spine number/10 microns) at 30 microns away from the cell body in KO animals. [MSN = medium spiny neuron; WT = wild-type; KO = dopamine transporter knockout].

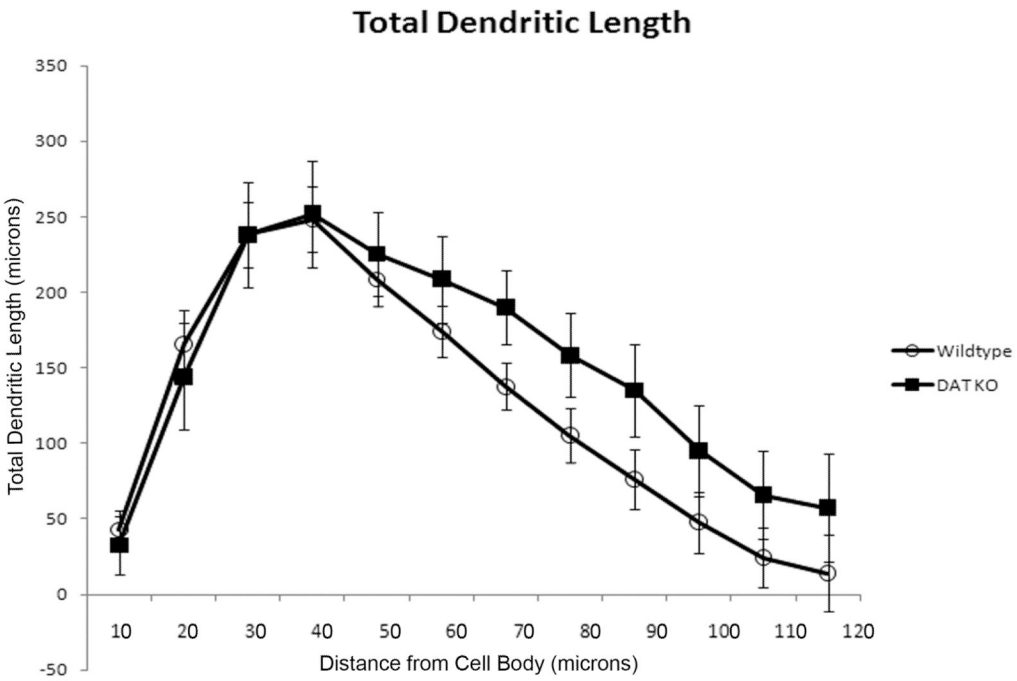

Figure 3. Total MSN dendritic length is not significantly different in DAT KO mice

Measurements of total dendritic length collected from a morphometric analysis comparing MSN cell tracings from WT and KO animals. No significant differences were found in total dendritic length between KO and WT mice. [MSN = medium spiny neuron; WT = wild-type; KO = dopamine transporter knockout].

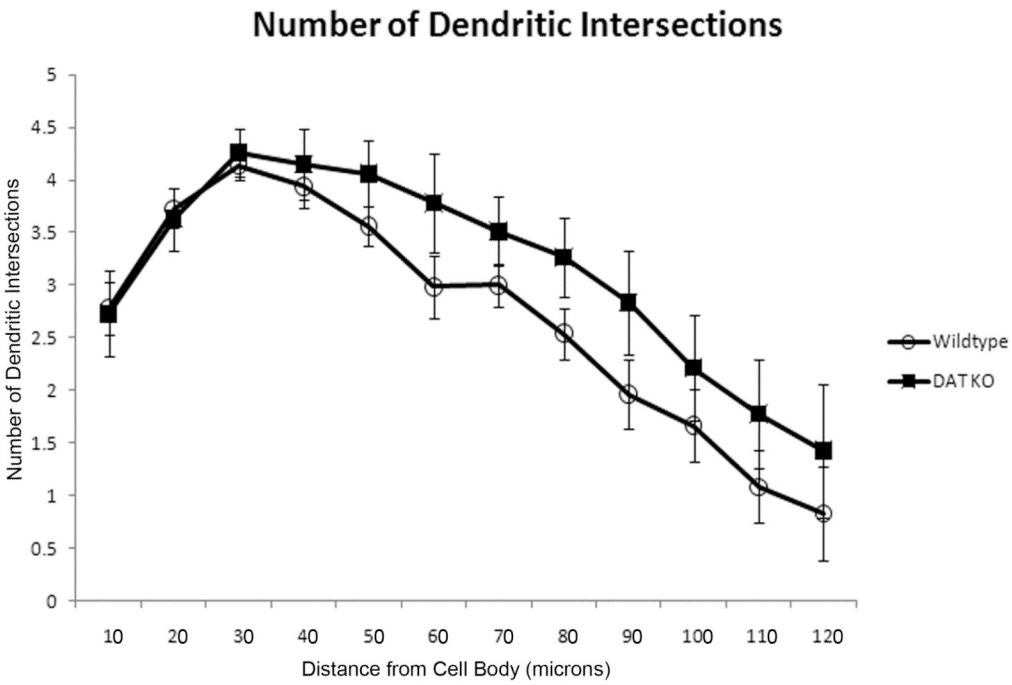

Figure 4. Dendritic intersections are not significantly different in DAT KO mice

Number of dendritic intersections collected from a morphometric analysis comparing MSN cell tracings from WT and DAT KO animals. The number of dendritic intersections between WT and KO animals was not significantly different. [MSN = medium spiny neuron; WT = wild-type; KO = dopamine transporter knockout].

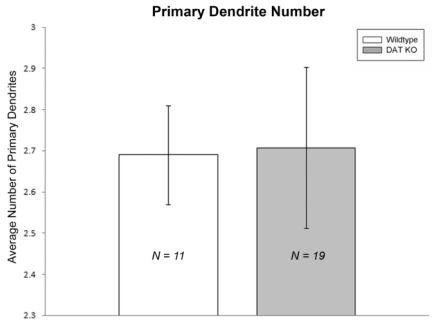

Figure 5. No alterations in DAT KO MSN primary dendrites

Bar graphs comparing the number of primary dendrites between groups. No significant differences were found between DAT KO and WT mice. [MSN = medium spiny neuron; WT = wild-type; KO = dopamine transporter knockout].

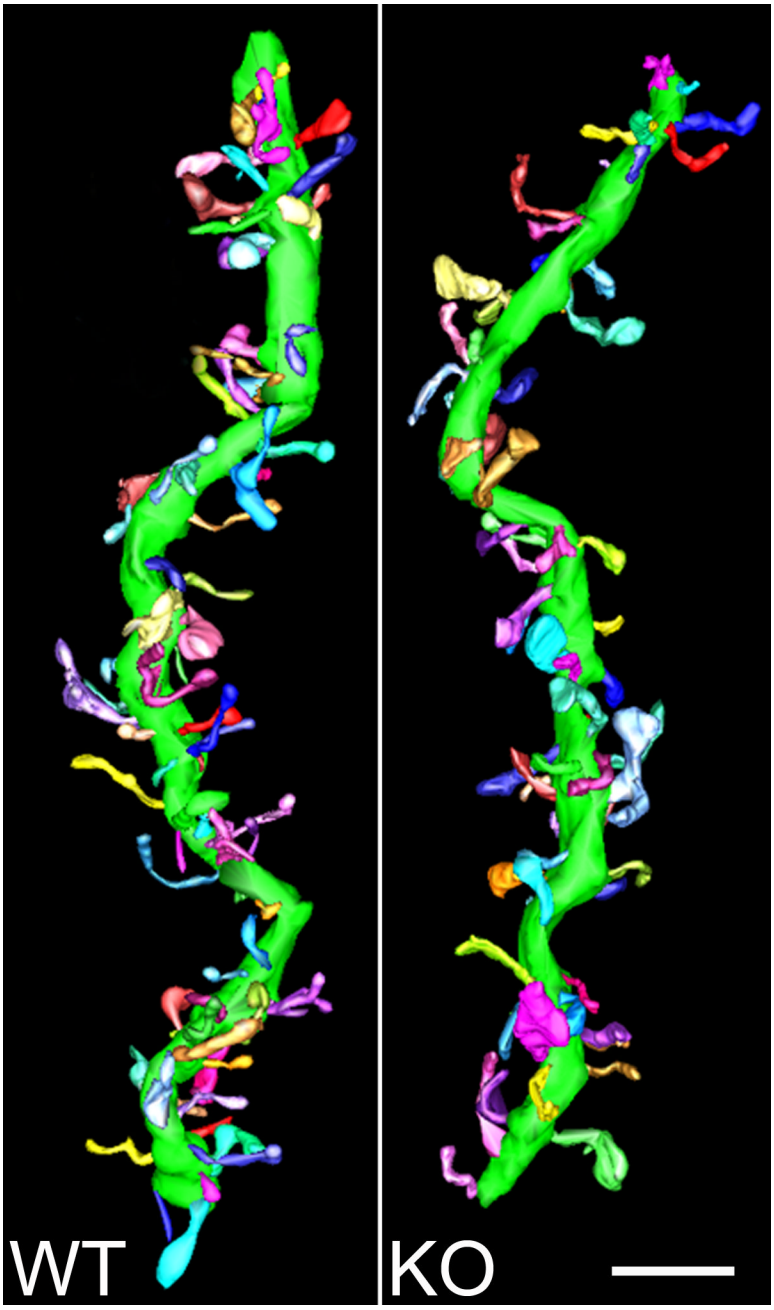

Figure 6. 3D rendered dendritic segments from EMT volumes

A representative dendritic segment from each group is shown. 3D-models were reconstructed using IMOD image modeling software [EMT = electron microscopic tomography; WT = wild-type; KO = dopamine transporter knockout; Scale bar = 2 microns].

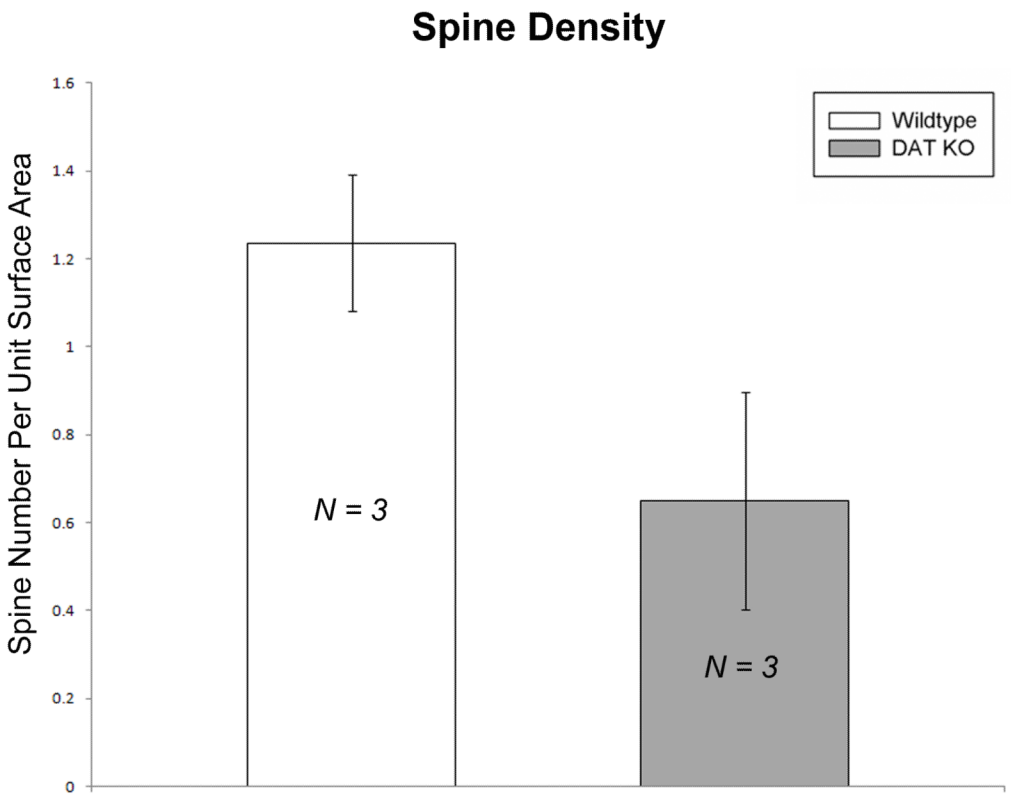

Figure 7. MSN spine density using EMT volumes is slightly decreased in DAT KO mouse

Bar graphs comparing the spine density (number of spines per unit surface area) between groups. A moderate decrease (did not reach statistical significance) in spine density was recorded between KO and WT mice. [MSN = medium spiny neuron; WT = wild-type; KO = dopamine transporter knockout].

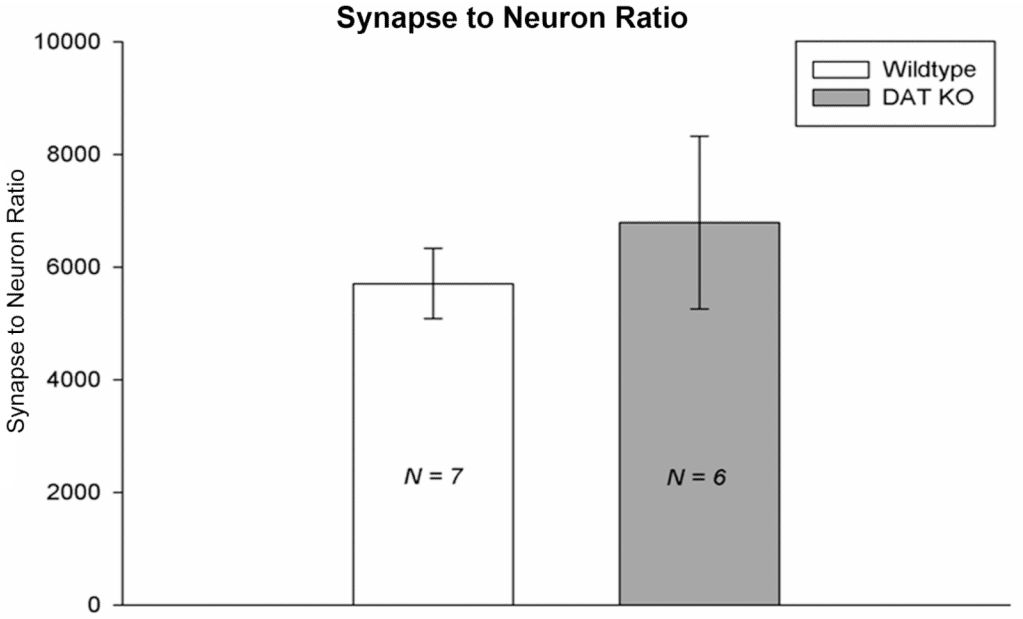

Figure 8. No change in DAT KO striatal synapse to neuron ratio

Bar graphs comparing the synapse to neuron ratio between groups. No significant differences were found between KO and WT mice. [WT = wild-type; KO = dopamine transporter knockout].

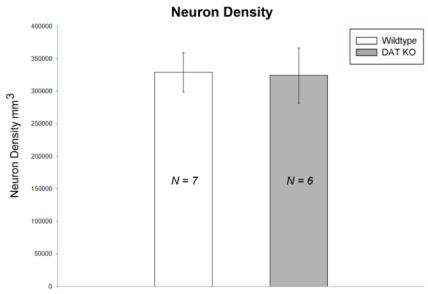

Figure 9. Striatal neuron cell density is not altered in DAT KO

Bar graphs comparing striatal neuron density between groups. Neuron density was found to be stable. No significant differences were found between DAT KO and WT mice. [WT = wild-type; KO = dopamine transporter knockout].